Electronic Supplementary Material (ESI) for Chemical Science.

Supplementary Information for

Thermal-induced Intermetallic Rh_1Zn_1 Nanoparticles with High Phase-purity for Highly Selective Hydrogenation of Acetylene

Xiaocheng Lan‡, Yu Wang‡, Boyang Liu, Zhenyu Kang, and Tiefeng Wang*

Beijing Key Laboratory of Green Reaction Engineering and Technology, Department of Chemical Engineering, Tsinghua University

Experimental Procedures

Catalyst preparation

All monometallic samples were prepared by incipient wetness impregnation using commercial SiO_2 (Alfa Aesar, 147 m^2/g) as the support. The RhO_x/SiO_2 was prepared with H_3RhCl_6 as the precursor. H_3RhCl_6 aqueous solution was prepared with a 3:1 molar ratio of HCl to $RhCl_3$ (99.9%, Alfa Aesar) and was added to the SiO_2 support with stirring. The mixture was sonicated for 1 h and then dried at 80 °C overnight. The dried sample was calcined in air at 400 ºC for 2 h. For ZnO/SiO_2, PtO_x/SiO_2, and PdO_x/SiO_2, the synthesis procedure was similar except that the metal precursor was $Zn(NO_3)_2{\cdot}6H_2O$ (Alfa Aesar), $H_2PtCl_6{\cdot}6H_2O$ (Alfa Aesar), and H_2PdCl_4 (prepared with a 2:1 molar ratio of HCl to $PdCl_2$), respectively. The metal loading of MO_x/SiO_2 for preparing M-Zn/SiO_2 (M = Rh, Pt, Pd) by Zn-ETO was 5.0%. The Rh metal loading of RhO_x/SiO_2 for preparing the Rh-Zn/SiO_2-t catalysts by Zn-ETO was 0.5%. The Zn metal loading of ZnO/SiO_2 for preparing the Rh-Zn/SiO_2-t catalysts by Zn-ETO was 2.0%. RhZn/SiO_2-IMP (with a Rh metal loading of 0.5% and a 1:1 molar ratio of Rh to Zn) was prepared by co-impregnation. H_3RhCl_6 and $Zn(NO_3)_2{\cdot}6H_2O$ aqueous solutions were premixed and added to the SiO_2. The mixture was sonicated for 1 h, dried at 80 °C overnight, calcined in air at 400 ºC for 2 h, and reduced at 400 °C for 4 h.

Characterization

HAADF-STEM and EDX images were obtained using a transmission electron microscope (FEI Titan Cubed G2 300) at 300 kV equipped with an aberration corrector for the probe-forming optics. All samples were ultrasonically dispersed in ethanol for 30 min and then dropped onto a carbon film supported on a copper grid. The particle size distribution was obtained by collecting more than 100 particles. XPS analysis of the reduced catalysts were performed on a Thermo-Fisher ESCALAB 250Xi instrument with an Al Kα X-ray source. For XPS and HAADF-STEM characterizations, the reduced samples were kept in vacuum condition before measurement to prevent oxidation. In situ XRD patterns were obtained on a Bruker D8 Advance diffractometer using CuKα radiation at 40 kV with a scanning rate of 1°/min. All MO_x/SiO_2 (M = Rh, Pt, Pd) samples were mixed with commercial ZnO (Alfa Aesar) and placed on the in situ plate for XRD analysis. The temperature program had four stages: in the first stage, the temperature was ramped to and kept constant at 300 °C for 1 h to simulate the metal reduction stage; in the second stage, it was ramped to and kept constant at 400 °C for 4 h to investigate the trapping and ordering process; in the third and fourth stages, it was ramped and kept constant at 500 °C and 600 °C for 2 h, respectively, to investigate the temperature effect on the trapping and ordering process. Each XRD scan was carried out for 20 min during the constant temperature section, and the samples were directly tested without taking out to expose to air. The ramping rate was 0.2 °C/s and the reducing atmosphere was 10% H_2/He. CO-FTIR spectra were collected on a Nicolet Nexus 470 spectrometer (Thermo Scientific) equipped with a mercury cadmium telluride (MCT-A) detector and vacuum system. Spectra were obtained with a resolution of 4 cm^{-1} using 64 and 32 scans for the background and samples, respectively. The catalyst was mixed with blank SiO_2 support with a weight ratio of 1:1 and finely ground. A 15 mg portion of the mixed sample was pressed onto a tungsten mesh and set inside the measurement cell. The sample was pretreated at 400 °C in a reducing atmosphere (11.0 kPa and 20% H_2 with He balance) for 1 h, and then the cell was purged with He three times followed by being kept under vacuum for 0.5 h to remove impurities on the catalyst surface. Finally, the cell was filled with 10% CO gas (balanced with He), then evacuated until the pressure decreased below 5.0×10^{-3} Pa to collect the CO-FTIR spectra. TGA was performed with a TGA/DSC1/1600LF instrument with a heating rate of 10 °C/min under air flow.

Catalytic reaction

Acetylene hydrogenation was carried out in a quartz fixed bed reactor of 7 mm inner diameter equipped with a K type thermocouple inserted into the catalyst bed to measure the temperature. Fresh RhO_x/SiO_2 (0.1g) and ZnO/SiO_2 (0.1g) catalysts were well mixed and the mixed powder was loaded into the reactor tube. The sample was pretreated with the procedure for Zn-ETO and cooled to 80 °C under N_2 flow before the catalytic test, the samples after reduction process were directly tested without taking out to expose to air. Acetylene hydrogenation was carried out with a gas flow of 100 mL/min containing 1% C_2H_2, 15% H_2, and N_2 as the balance gas. The outlet stream was analyzed online by a gas chromatograph equipped with a FID detector and a HP-Al/S PLOT column, the details of which were given in our previous work.[1] The conversion of acetylene and the selectivities to ethylene, ethane, C_4, and GO were calculated as

$$S_{C_2H_4} = \frac{n_{C_2H_4}}{n_{C_2H_2,in} - n_{C_2H_2,out}} \times 100\%$$

$$S_{C_2H_6} = \frac{n_{C_2H_6}}{n_{C_2H_2,in} - n_{C_2H_2,out}} \times 100\%$$

$$S_{C_4} = \frac{2 \times n_{C_4}}{n_{C_2H_2,in} - n_{C_2H_2,out}} \times 100\%$$

$$S_{GO} = 1 - S_{C_2H_4} - S_{C_2H_6} - S_{C_4}$$

where $n_{C_2H_4}$, $n_{C_2H_6}$, n_{C_4} and $n_{C_2H_2,out}$ were the moles of each compound in the outlet gas, and $n_{C_2H_2,in}$ was the moles of acetylene in the inlet gas determined by a bypass run prior to each test.

Computational calculation

The Zn-ETO process and C_4 formation were studied by DFT calculations with the Vienna Ab initio Simulation Package (VASP).[2-3] Electron-ion and electron-electron interactions were described by the projected augmented wave (PAW) method[4-5] and the Perdew-Burke-Ernzerhof (PBE) exchange-correlation functional[6], respectively. A 400 eV kinetic cutoff energy and 0.1 eV Gaussian smearing width were set for structure optimization and the transitional state search. The Brillouin zone was sampled with 3×3×1 Monkhorst-Pack k-point mesh. Transitional states were optimized with the climbing image nudged elastic band (CI-NEB) method.[7] Projected density of states (PDOS) and d-band cneter of Rh(111) and RhZn(110) surfaces were calculated using 2001 points. Bader charge analysis was employed to calculate the charge partitioning. The ZnO, Rh and RhZn crystal structures were obtained from Materials Project.[8] For the reaction calculation, a 2×2 supercell and 3 layer slab model were used to simulate C_4 formation, with at least 20 Å vacuum between slabs to exclude vertical interactions. The top two layers were relaxed and the bottom layer was fixed to represent the bulk phase. For the Zn-ETO process, the energy change due to Zn evaporation was calculated using a ZnO (221) surface and a 2×1 supercell was applied. VASPKIT[9] was used for the calculation of the Gibbs free energy.

For C_4 formation, the adsorption energy was calculated as

$$E_{ads} = E_{surface+adsorbate} - E_{surface} - E_{adsorbate}$$

where $E_{surface+adsorbate}$ was the calculated energy of the surface with adsorbate on it, and $E_{surface}$ and $E_{adsorbate}$ were the calculated energies of the bare surface and gaseous adsorbate (reactant or product), respectively.

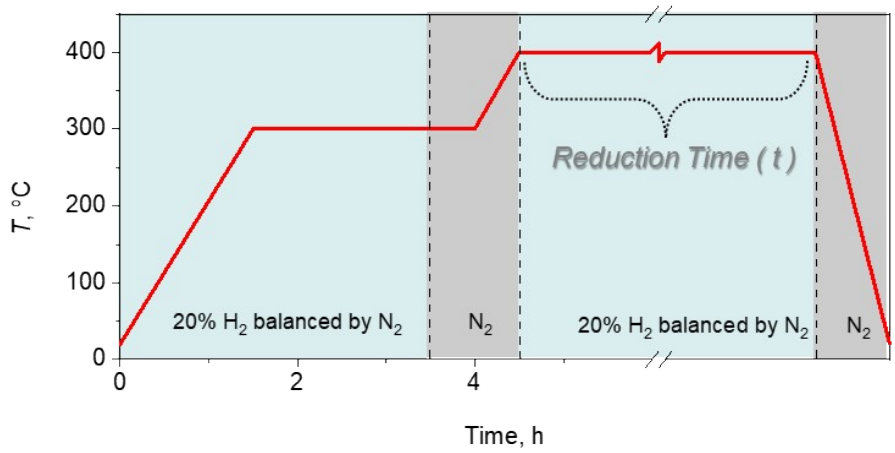

Figure S1. The temperature programmed reduction procedure. The temperature was first set to 300 °C for 2 h with 50 ml/min of 20% H_2 gas balanced by N_2 and then increased to 400 °C for a reduction time of *t* h.

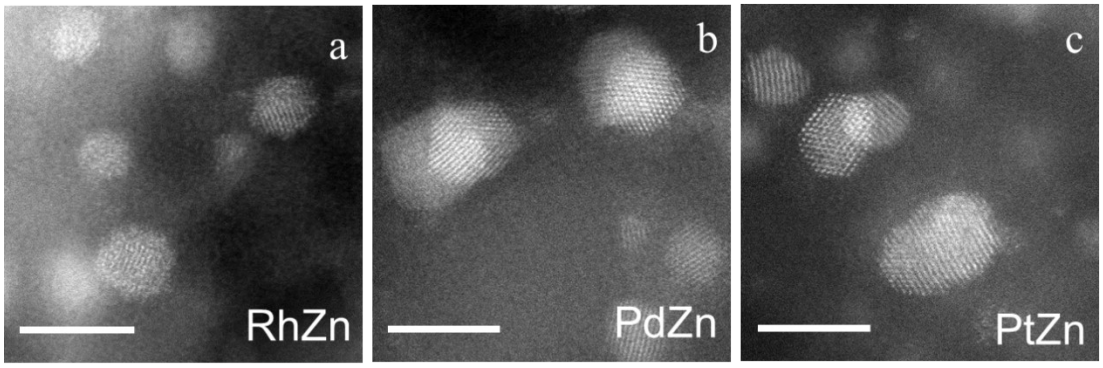

Figure S2. HAADF-STEM images of (a) Rh-Zn/SiO_2, (b) Pd-Zn/SiO_2, and (c) Pt-Zn/SiO_2. All scale bars in this figure are 5 nm.

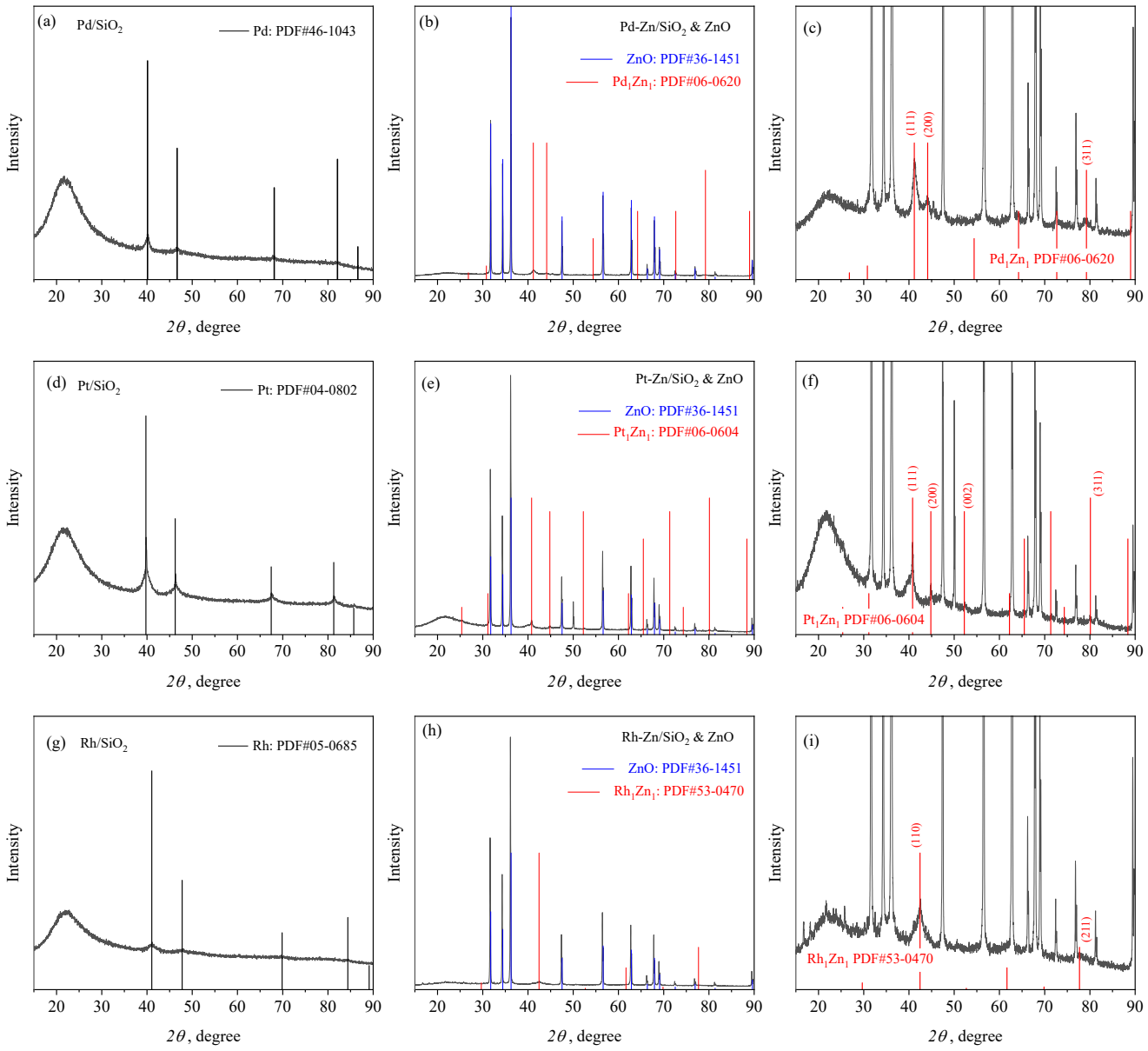

Figure S3. XRD patterns of Pd/SiO_2 (a), $Pd\text{-}Zn/SiO_2$ (b and c), Pt/SiO_2 (d), $Pt\text{-}Zn/SiO_2$(e and f), Rh/SiO_2 (g), and $Rh\text{-}Zn/SiO_2$ (h and i). The patterns in c, f and i are the enlarged patterns of b, e and f.

(a)

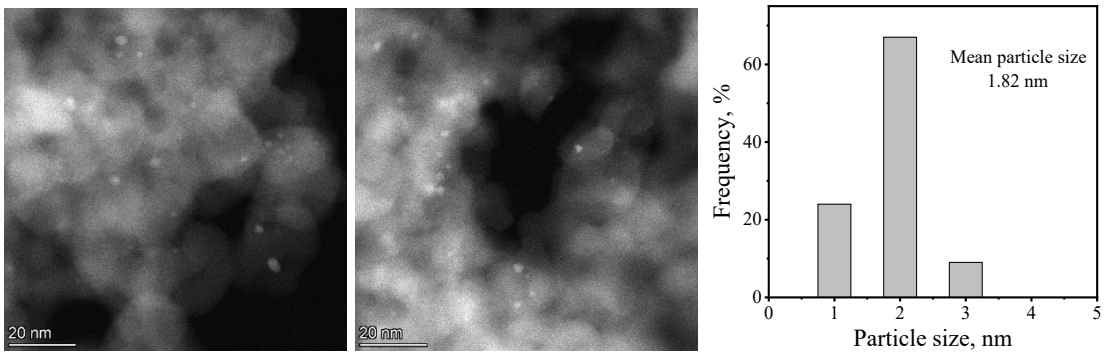

(b)

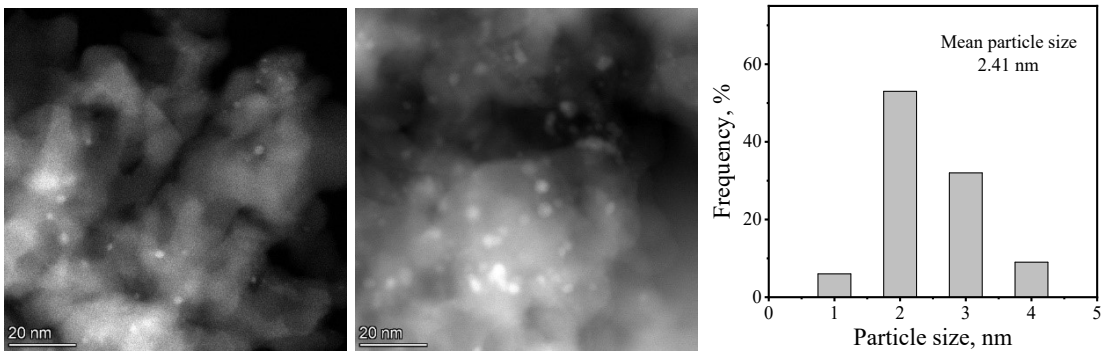

Figure S4. HAADF-STEM images of the catalysts. a, Rh-Zn/SiO_2-0. b, Rh-Zn/SiO_2-10

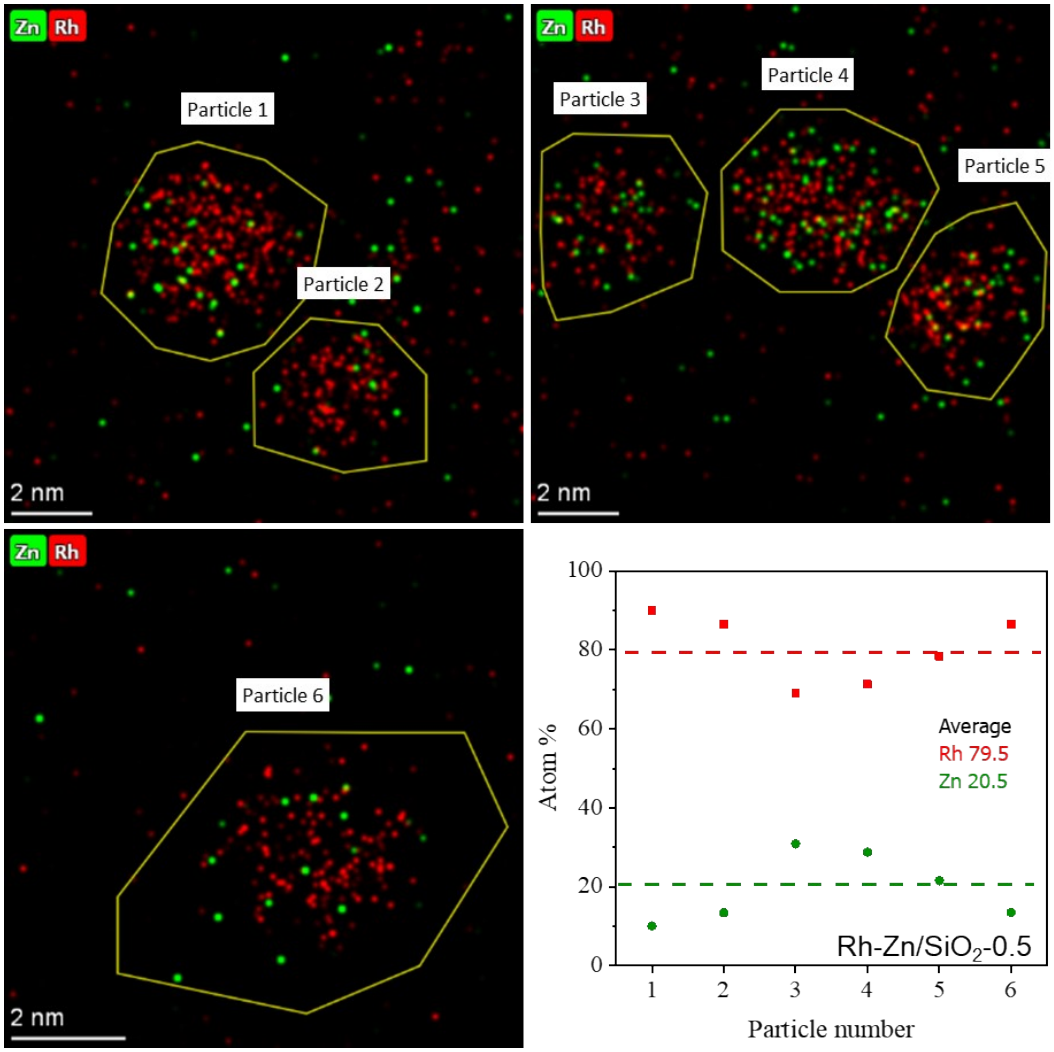

Figure S5. STEM-EDS analysis of Rh-Zn/SiO_2-0.5

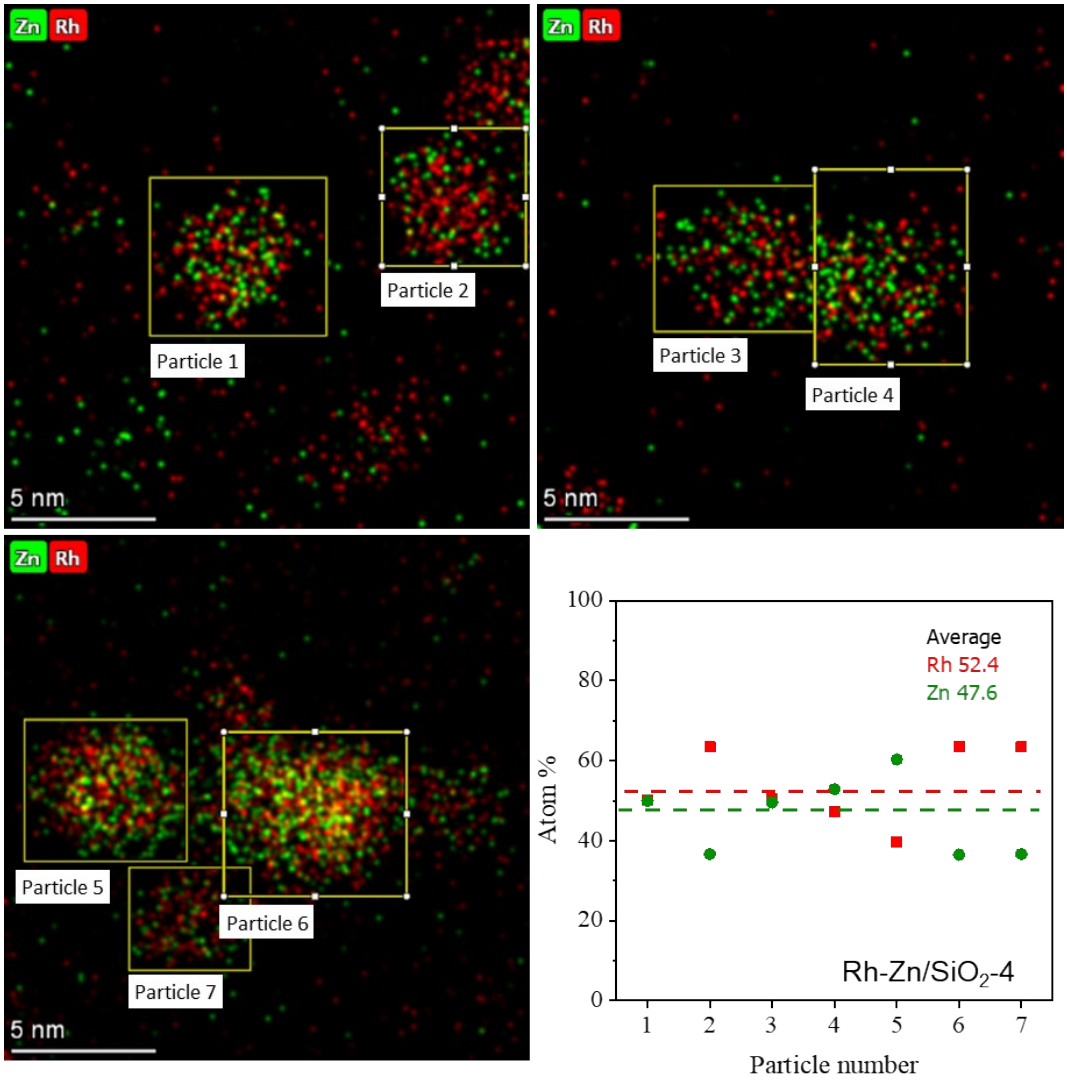

Figure S6. STEM-EDS analysis of Rh-Zn/SiO_2-4

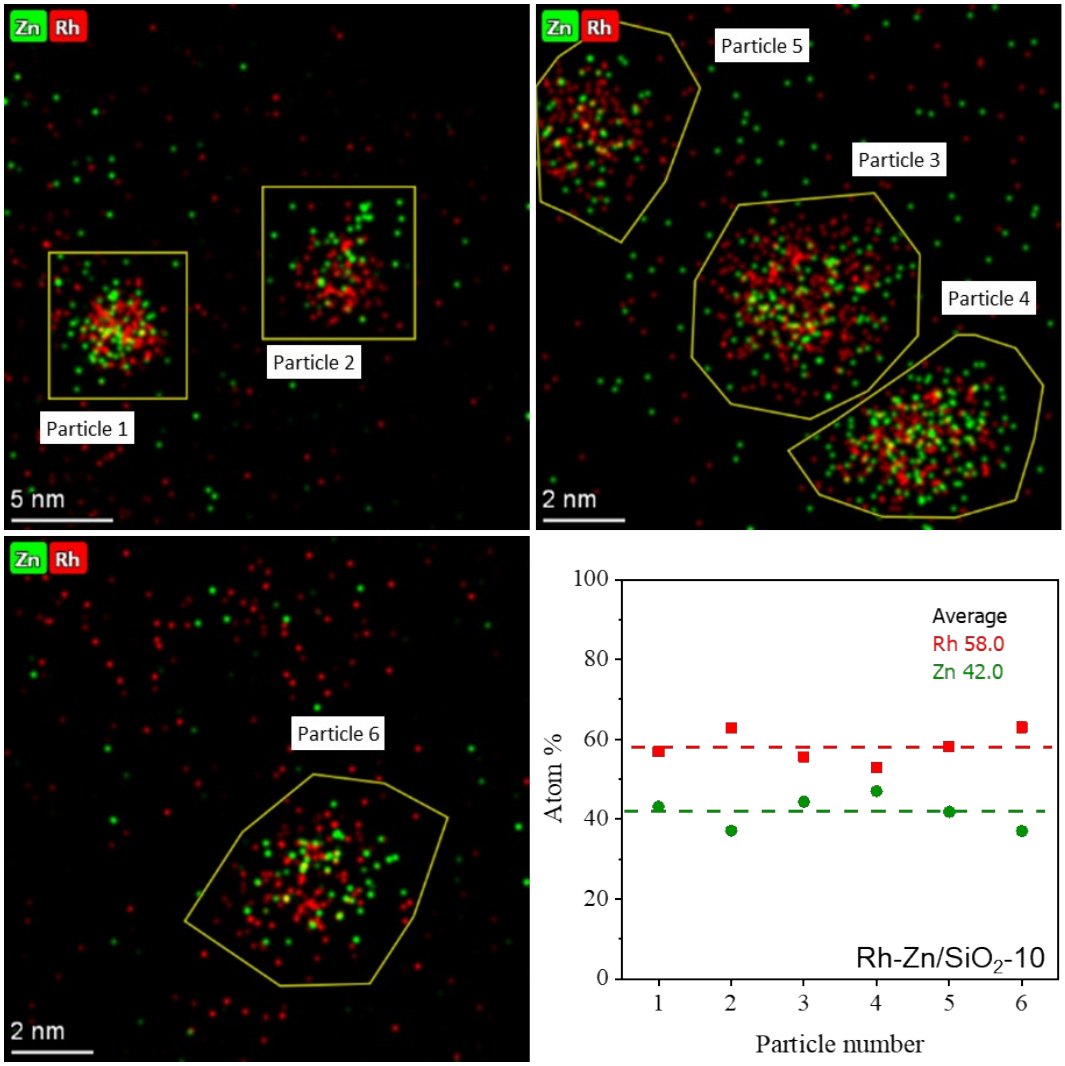

Figure S7. STEM-EDS analysis of Rh-Zn/SiO_2-10

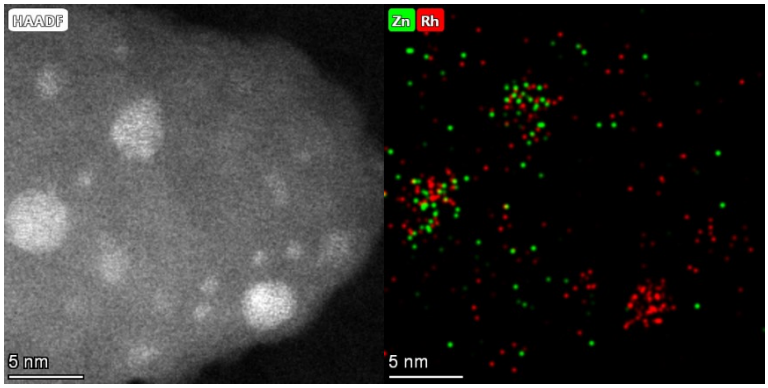

Figure S8. HAADF-STEM and EDX images of $RhZn/SiO_2$-IMP.

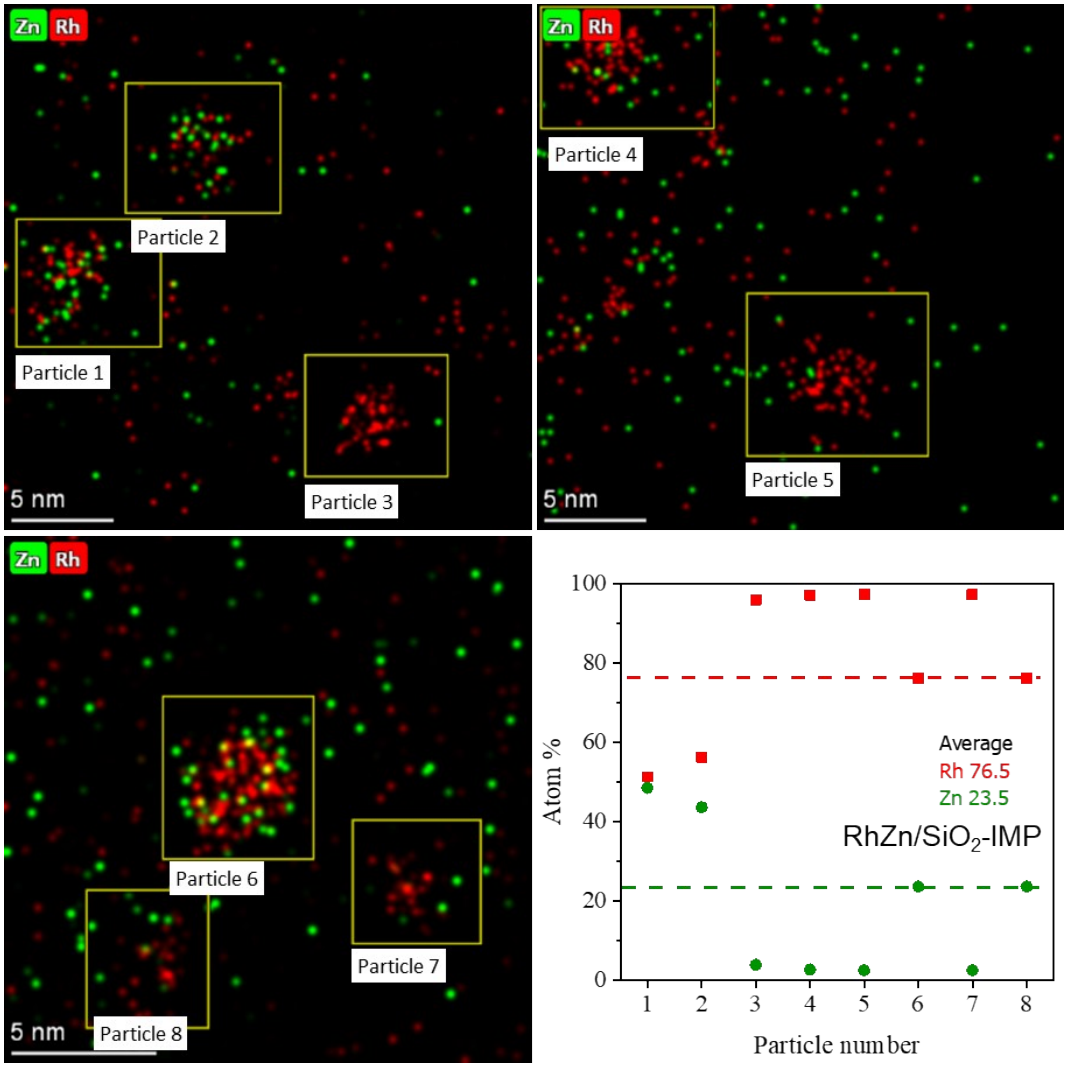

Figure S9. STEM-EDS analysis of RhZn/SiO_2-IMP.

(a)

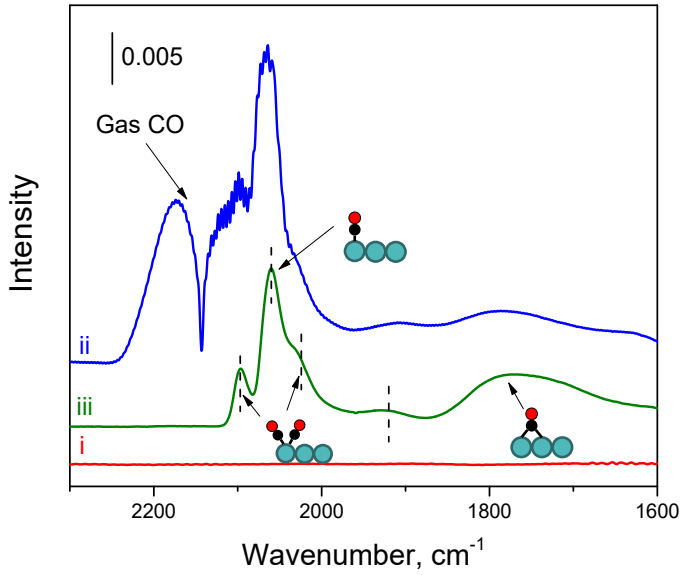

(b)

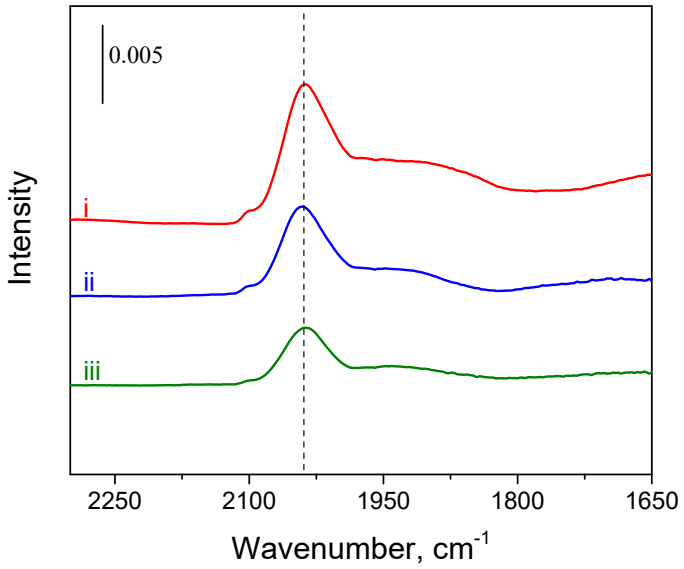

Figure S10. FTIR spectra of the catalysts after CO adsorption. a, FTIR spectra of Rh-Zn/SiO_2-0, before adding CO (i), adding 10% CO at ~5 kPa (ii), and after evacuating to 5.0×10^{-3} Pa (iii). b, CO adsorption over RhZn/SiO_2-IMP reduced at 400 °C for 2 h (i), 4 h (ii), and 10 h (iii). Each CO-FTIR characterization used the same procedure (i-iii) of Rh-Zn/SiO_2-0 in Figure S9a. The FTIR spectra of CO adsorption for RhZn/SiO_2-IMP in Figure S9b were obtained after evacuation to 5.0×10^{-3} Pa.

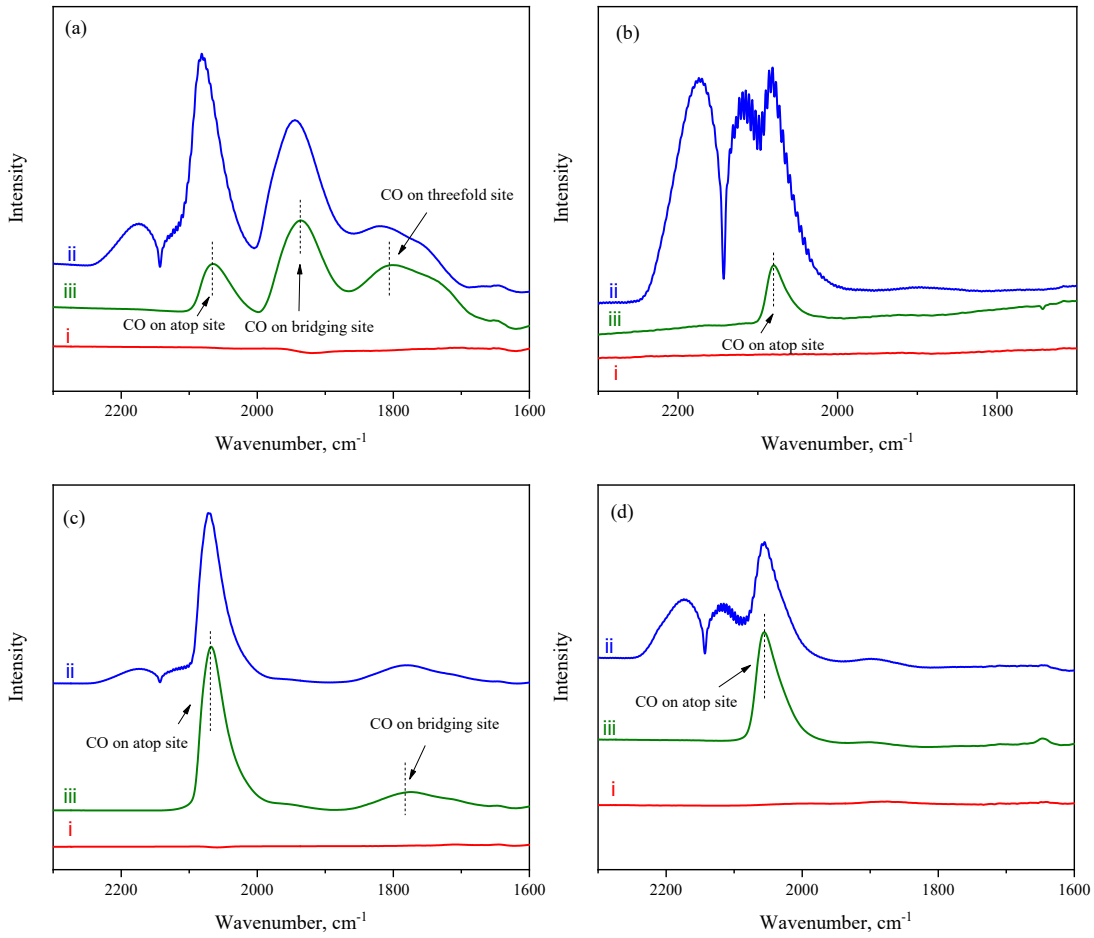

Figure S11. CO-FTIR spectra of Pd/SiO_2 (a), $Pd\text{-}Zn/SiO_2$ (b), Pt/SiO_2 (c) and $Pt\text{-}Zn/SiO_2$ (d). Before adding CO (i), adding 10% CO at ~5 kPa (ii), and after evacuating to 5.0×10^{-3} Pa (iii). The IR spectrum of Pd/SiO_2 contained a large peak at 1940 cm^{-1} and a smaller peak at 2066 cm^{-1} which corresponded to the CO adsorbed on bridging site and atop site on Pd, respectively. In addition, Pd/SiO_2 exhibited a broad peak of CO adsorbed on threefold Pd site at 1800 cm^{-1}. By trapping Zn atoms, the Pd_1Zn_1 intermetallic phase was formed. The isolated Pd sites favored CO adsorption on atop sites for, and thus the IR spectrum of $Pd\text{-}Zn/SiO_2$ only exhibited the peak of CO adsorbed on atop site. Similarly, compared with Pt/SiO_2, $Pt\text{-}Zn/SiO_2$ only showed the peak of CO on atop site.

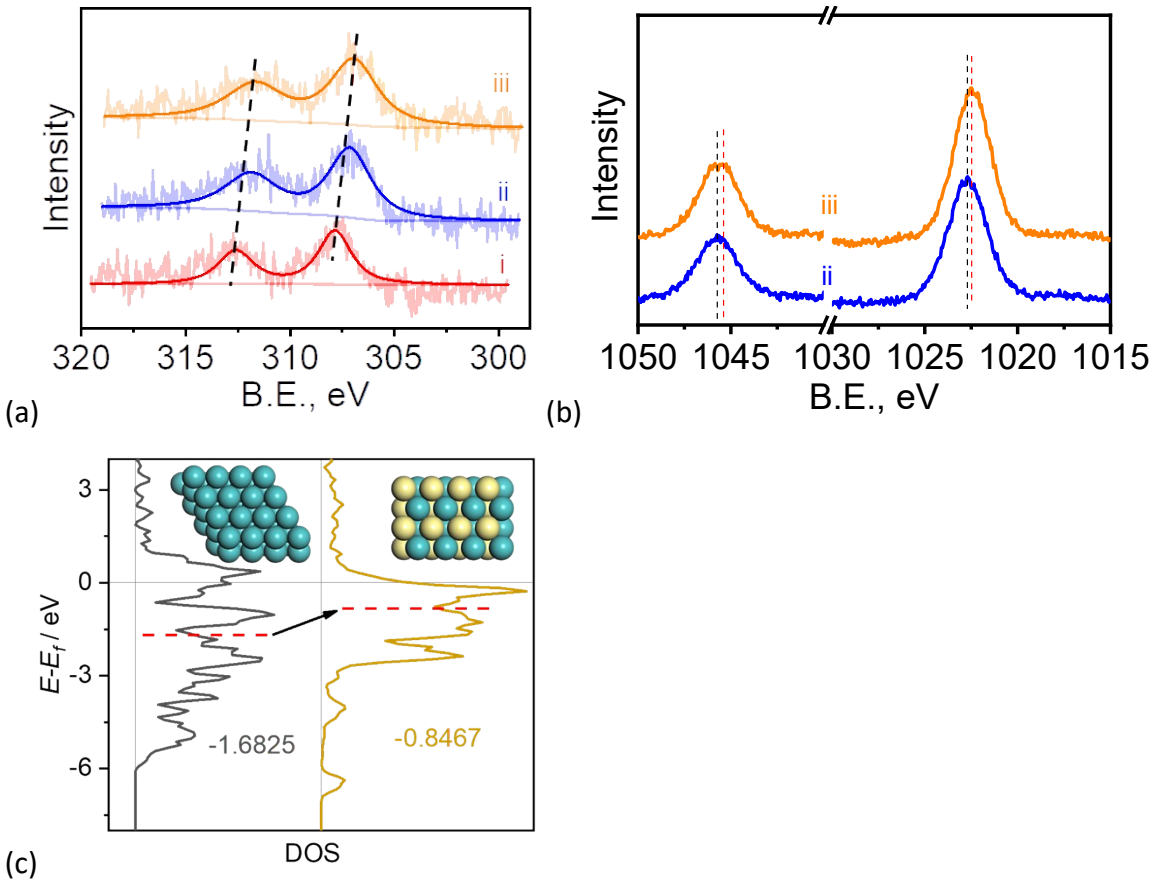

Figure S12. (a)Rh 3d and (b) Zn 2p XPS analysis of Rh-Zn/SiO_2-0 (i), Rh-Zn/SiO_2-0.5 (ii), and Rh-Zn/SiO_2-4 (iii). (c) d-band center of Rh and Rh_1Zn_1.

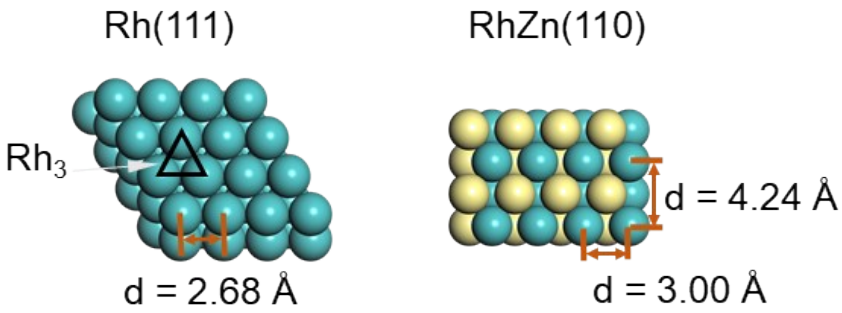

Figure S13. Surface Rh atom distribution over Rh(111) and RhZn(110).

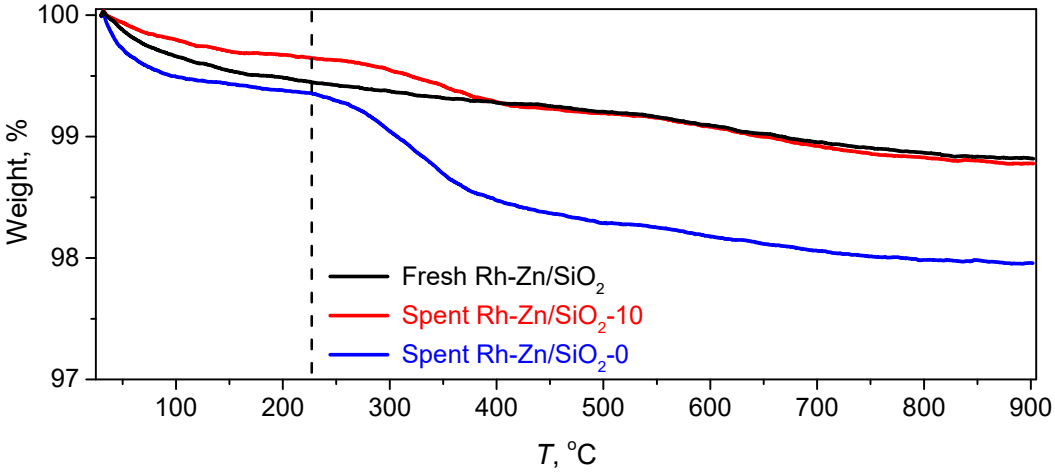

Figure S14. TGA results of fresh and spent catalysts. Spent Rh-Zn/SiO_2-10 and spent Rh-Zn/SiO_2-0 were the catalysts after evaluation by the temperature programmed reaction in Figure 1. Fresh catalyst Rh-Zn/SiO_2 was treated by the same reduction procedure as Rh-Zn/SiO_2-0.

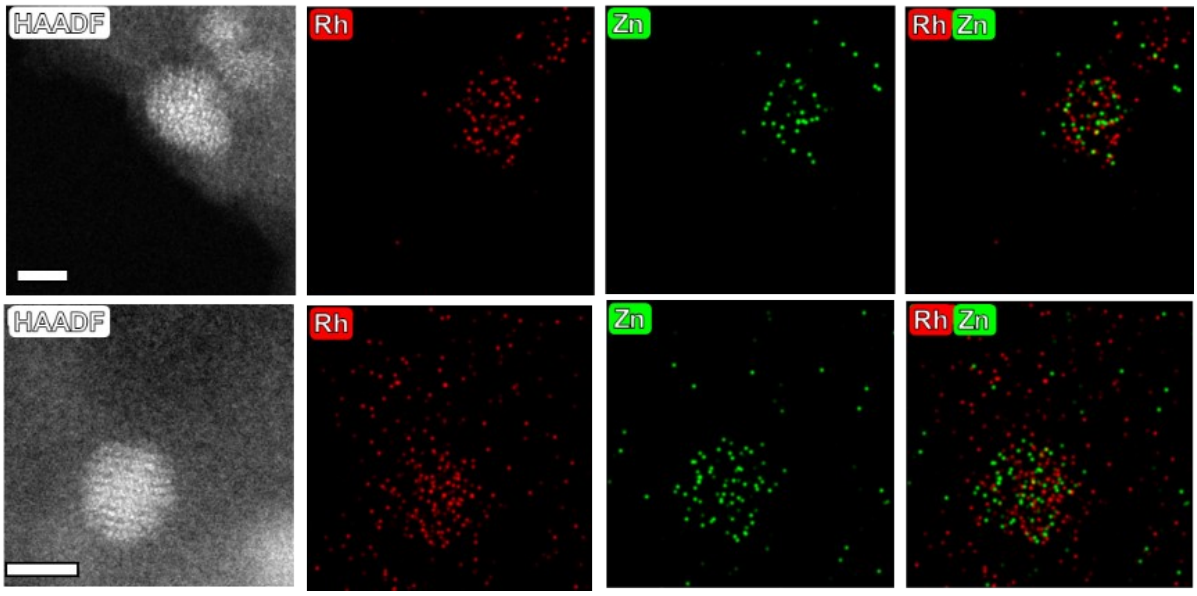

Figure S15. HAADF-STEM images and EDS mappings of the spent Rh-Zn/SiO_2-10.

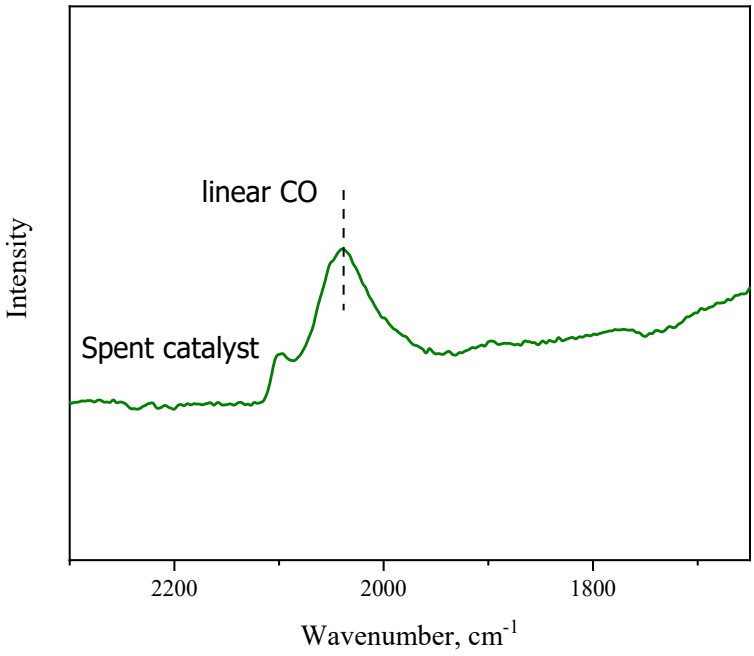

Figure S16. CO adsorption on the spent Rh-Zn/SiO_2-10.

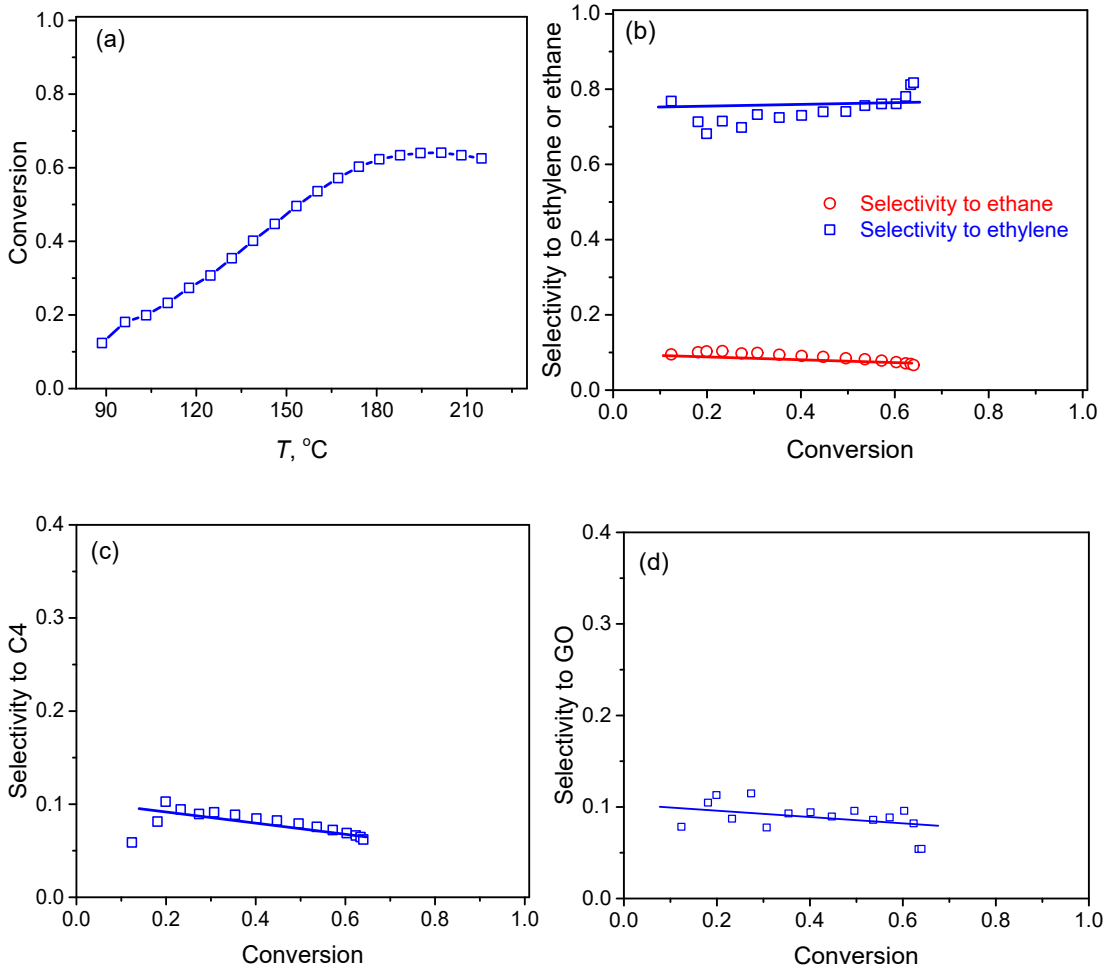

Figure S17. Acetylene hydrogenation over $RhZn/SiO_2$-IMP. a, Acetylene conversion during the temperature programmed reaction. b-d, Selectivity to ethylene (b), ethane (b), C_4 (c) and GO (d) versus acetylene conversion. 0.1 g $RhZn/SiO_2$-IMP catalyst was mixed with 0.1 g blank SiO_2 and reduced at 400 °C for 2 h before evaluation. The temperature programmed reaction was performed under the same conditions as Rh-Zn/SiO_2-*t*.

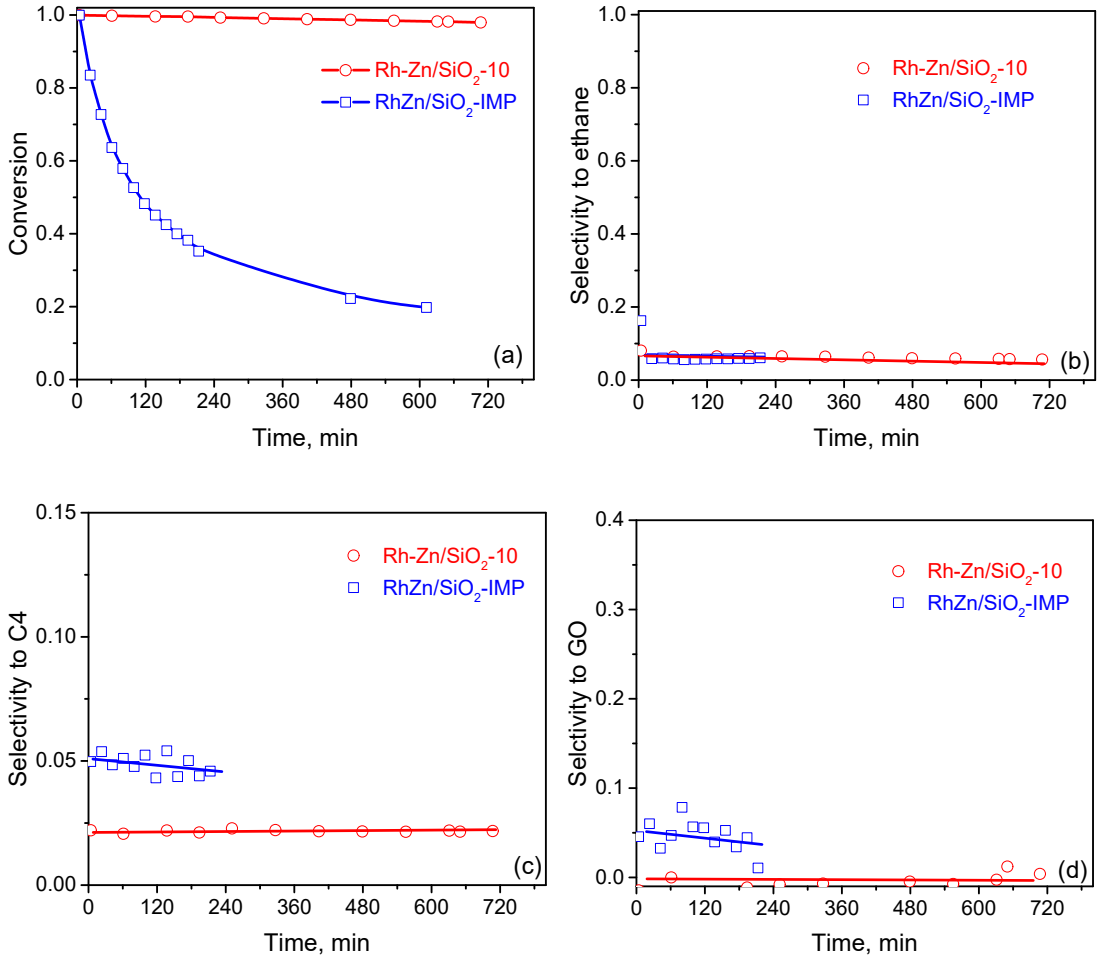

Figure S18. Catalyst stability evaluation of Rh-Zn/SiO_2-10 and RhZn/SiO_2-IMP. a, Acetylene conversion during stability evaluation. b-d, Selectivity to ethane (b), C_4 (c) and GO (d) during stability evaluation. Catalyst stability was evaluated at 217 °C with a gas flow of 100 mL/min containing 1% C_2H_2, 15% H_2, and N_2 as the balance gas. For RhZn/SiO_2-IMP, 0.1 g RhZn/SiO_2-IMP sample was mixed with 0.1 g blank SiO_2 and reduced at 400 °C for 2 h before evaluation. For Rh-Zn/SiO_2-10, 0.1 g Rh/SiO_2 was mixed with 0.1 g ZnO/SiO_2 and treated by TPR for 10 h before evaluation.

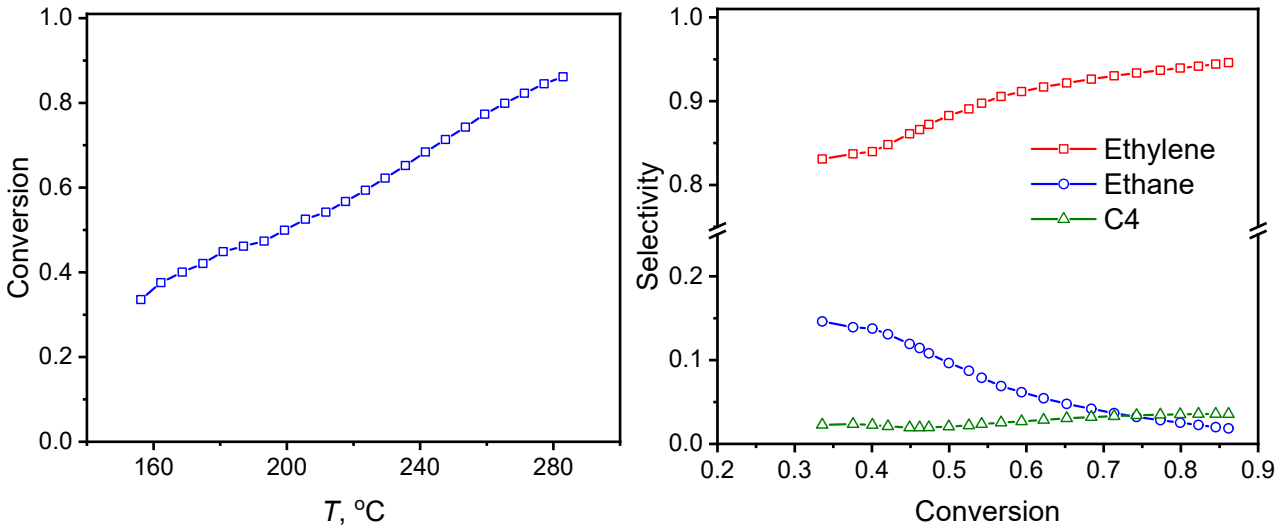

Figure S19. Catalytic performance of Rh-Zn/SiO_2-4 catalysts in acetylene hydrogenation under the feed condition of 1% C_2H_2, 20% C_2H_4, and 4% H_2.

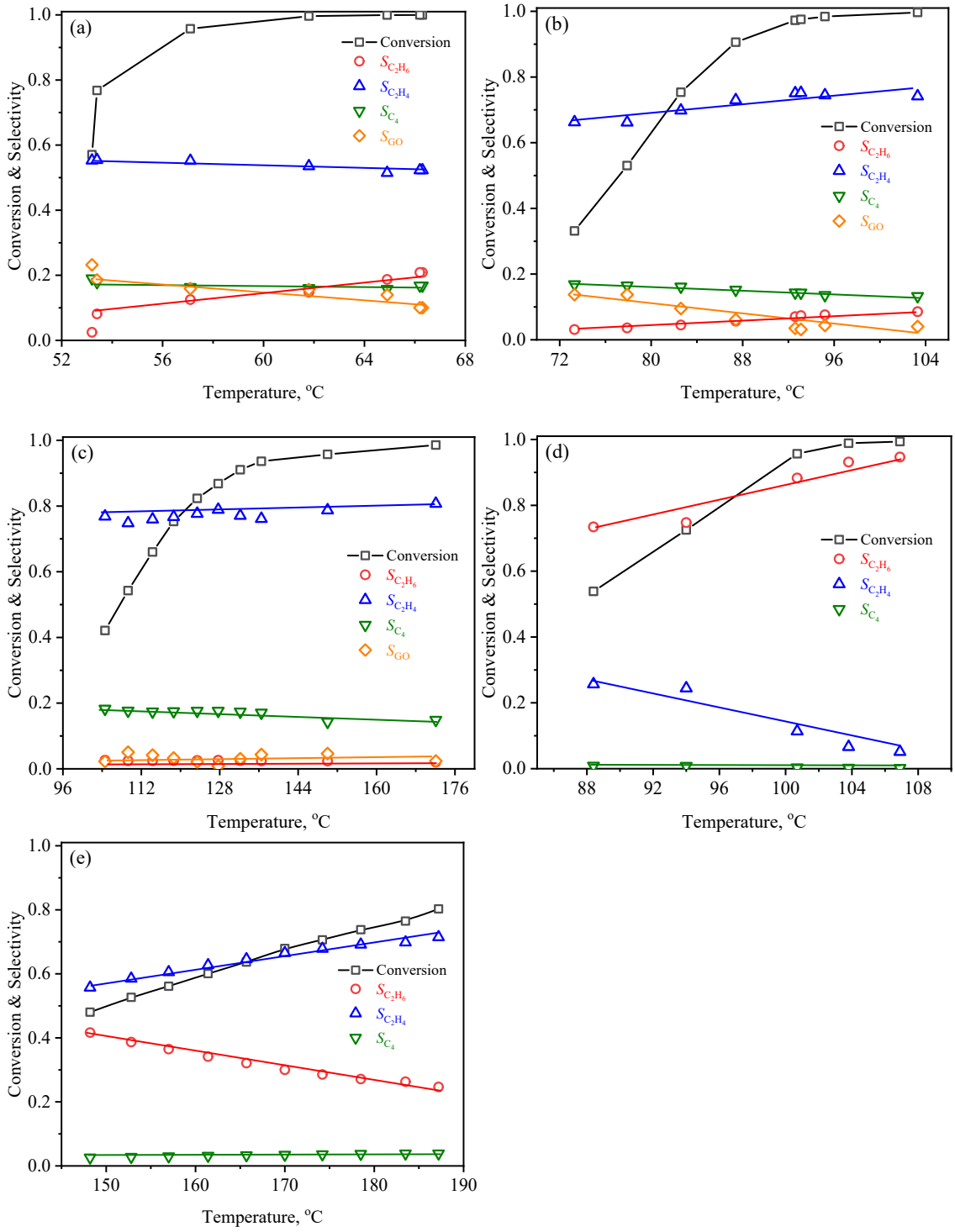

Figure S20. Reduction time dependent catalytic performance of Pd-Zn/SiO_2-t catalysts in acetylene hydrogenation. (a) Pd-Zn/SiO_2-0, (b) Pd-Zn/SiO_2-2, (c) Pd-Zn/SiO_2-4, (d) Pt-Zn/SiO_2-0, and (e) Pt-Zn/SiO_2-4.

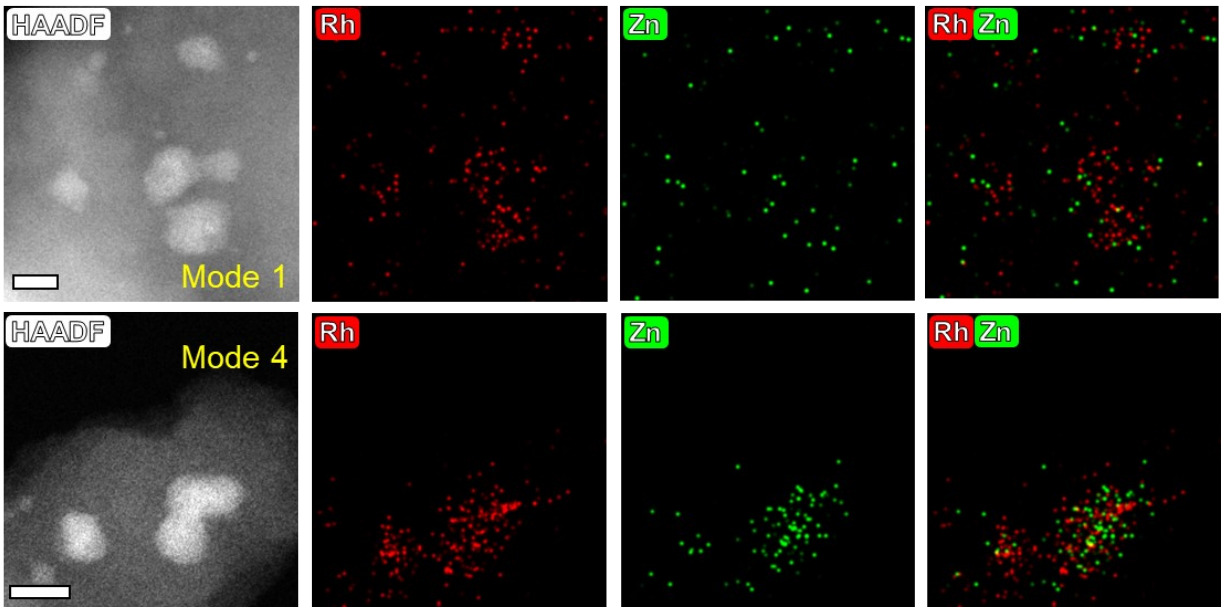

Figure S21. HAADF-STEM images and EDS mappings of samples in mode 1 and 4 after TPR process.

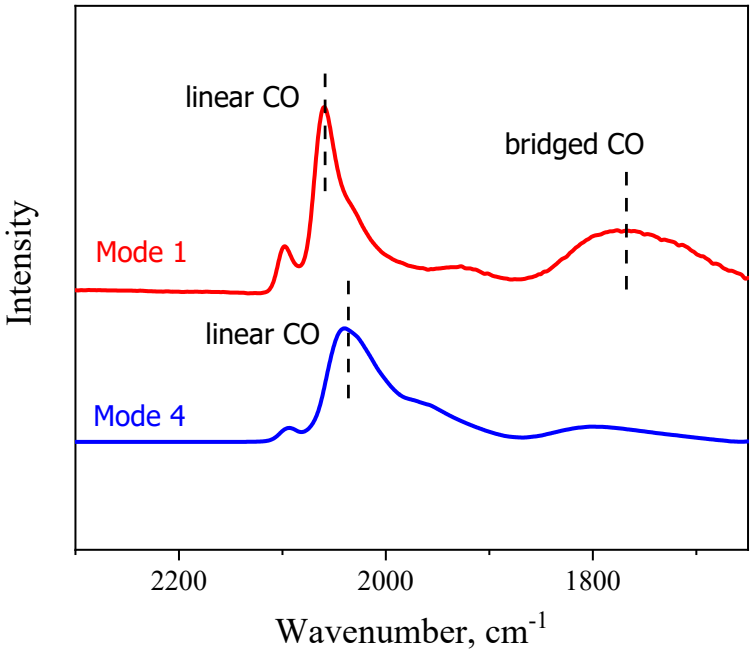

Figure S22. CO adsorption on the samples in mode 1 and 4 after TPR process.

Table S1. Comparison of the present catalysts with the reported intermetallic and alloy catalysts for acetylene semihydrogenation.

Entry	Cat	Active Phase	Temp °C	Feeding ratio[a]	Conv %	Cal Method[b]	S(C_2H_4) %	S(C_4) %[c]	Carbon loss of C_2H_2, %[d]	Ref
1	Ni_3Sn	Ni_3Sn	250	1:5:0	100	--	68	30	NR	10
2	Ni_3Ge/MCM-41	Ni_3Ge	250	1:2:0	94	--	89	8.4	0.1	11
3	PdGa	PdGa	120	1:2:0	50	A	80	NR	NC	12
4	PdGa	PdGa	200	1:10:100	86	B	75	NR	NC	12
5	PdGa	PdGa	200	1:10:100	66	B	76	NR	NC	13
6	Pd_2Ga	Pd_2Ga	200	1:10:100	94	B	75	NR	NC	13
7	nano-PdGa@Al_2O_3	PdGa	200	1:10:100	81	B	82	NR	NC	13
8	nano-Pd_2Ga@Al_2O_3	Pd_2Ga	200	1:10:100	88	B	66	NR	NC	13
9	Fe_4Al_{13}	Fe_4Al_{13}	200	1:10:100	81	B	84	10	NC	14
10	Pd/ZnO	Pd_1Zn_1	110	1:10:0	100	E	77	14	4	15
11	Pd/ZnO	Pd_1Zn_1	110	1:10:20	78	D	91	NR	NC	15
12	$InPd_2$	$InPd_2$	200	1:10:100	90	B	80	NR	NC	16
13	$GaPd_2$	$GaPd_2$	200	1:10:100	95	B	75	NR	NC	16
14	Ni_3Ga	Ni_3Ga	200	1:20:100	91	B	77	11	NC	17
15	Ni_3Sn_2	Ni_3Sn_2	200	1:20:100	74	B	80	10	NC	17
16	PdIn/$MgAl_2O_4$	PdIn	90	1:10:100	95	B	90	NP	NC	18
17	NiGa	NiGa	240	1:10:0	90	C	82	NP	NC	19
18	$Ni_3ZnC_{0.7}$/oCNT	$Ni_3ZnC_{0.7}$	200	1:9:0	100	E	~85	~9	~0	20
19	$Ni_3ZnC_{0.7}$/oCNT	$Ni_3ZnC_{0.7}$	200	1:9:40	99	D	95	NR	NC	20
20	Pd_1Ag_3/r-TiO_2	Pd_1Ag_3	70	1:10:100	96	D	85	NR	NC	21
21	Pd_1Ag_3/HT	Pd_1Ag_3	60	1:10:100	100	D	80	NR	NC	21
22	Ni_3Zn/oCNT	Ni_3Zn	160	1:15:0	40	E	70	8	10	1
23	$Ni_3ZnC_{0.7}$/C	$Ni_3ZnC_{0.7}$	160	1:15:0	100	E	85	4	<2	1
24	$Ni_3GaC_{0.5}$	$Ni_3GaC_{0.5}$	110	1:5:20	100	C	89.1	4.3	NC	22
25	Pd_3Bi/SiO_2	Pd_3Bi	150	1:4:0	90	D	80	NR	NC	23
26	NiSb	NiSb	240	1:5:60	100	C	93.2	3.6	NC	24
27	Pd_8Zn_{44}	Pd_8Zn_{44}	160	1:18:31	87	E	85	NR	NR	25
28	Pd_9Zn_{43}	Pd_9Zn_{43}	160	1:18:31	97	E	75	NR	NR	25
29	Pd_8AuZn_{43}	Pd_8AuZn_{43}	160	1:18:31	100	E	64	NR	NR	25
30	$CaPdH_2$	$CaPdH_2$	100	1:10:0	85	E	80	NR	NR	26
31	PdCu	B2	25	1:2:1	42	--	~75	~17	NC	27
32	PdCu	fcc	25	1:2:1	12	--	~70	~23	NC	27
33	Pd-Zn/SiO_2-4	Pd_1Zn_1	172	1:15:0	98	E	81	15	2	TW
34	Rh/SiO_2	Rh	150	1:15:0	79	E	52	25	13	TW
35	RhZn/SiO_2-IMP	Mix phase	217	1:15:0	83	E	83	5.4	6	TW

36	**Rh-Zn/SiO_2-10**	**Rh_1Zn_1**	**217**	**1:15:0**	**100**	**E**	**91**	**2.2**	**<0.5**	TW

[a] Volume ratio of C_2H_2:H_2:C_2H_4. [b] Five Calculation methods, denoted as A-E, are discussed below. [c] Reported C_4 selectivity, and "NR" for no report. [d] Reported carbon loss or carbon balance, and "NR" for no report, "NC" for non calculable.

Several calculation methods were used to determine the selectivity in the reported works (Table S1 and S2). Method A assumes that the hydrogenation products only contain ethylene, ethane, and C_4. For the acetylene hydrogenation in ethylene flow, since ethylene is in significant excess it is typically difficult to accurately detect the change of ethylene concentration coming from hydrogenation of 0.5~1% acetylene.[28-29] Methods B-D are proposed to indirectly calculate the ethylene selectivity by measuring ethane and C_4 (ethane and C_4 can be accurately measured because the feed does not contain these components). However, acetylene semihydrogenation is accompanied by oligomerization with the formation of GO components (deposited long chain hydrocarbons). GC for quantitative analysis only detects the light hydrocarbons of acetylene, ethylene, ethane, and C_4, while GO components are not vaporizable to be detected. The formula and the neglect of GO in Methods B-D could overrate the intrinsic selectivity to C_2H_4. It should be specifically noted that some works only considered the ethylene and ethane products and the formula of $S(C_2H_4)$ did not consider the by-products of C_4 and GO (Method D), which highly overrated the intrinsic selectivity to ethylene.

For the acetylene hydrogenation without ethylene, the change of ethylene concentration can be directly measured and thus the $S(C_2H_4)$ can be accurately calculated by Method E. For example, as listed in Table S1 (entry 10 vs 11, and 18 vs 19), the $S(C_2H_4)$ for Pd/ZnO was 91% calculated by method D (with excess ethylene in the feed) but was only 77% calculated by method E (without excess ethylene in the feed), and the $S(C_2H_4)$ for $Ni_3ZnC_{0.7}$/oCNT was 95% calculated by method D (with excess ethylene in the feed) but was only 85% calculated by method E (without excess ethylene in the feed).Recently, Method E was used to determine the $S(C_2H_4)$ in the feed with excess of ethylene by using two different isotopes ^{13}C and ^{12}C for ethylene and acetylene, respectively (entry 27-29).

In this work, we use method E to accurately determine the intrinsic selectivity to C_2H_4 under the feeding condition without excess ethylene. Our Rh_1Zn_1 catalyst obtained a high intrinsic selectivity to ethylene (91%) with extremely low C_4 and GO formation, which outperforms the reported intermetallic and alloy catalysts for acetylene semihydrogenation.

Table S2. The conversion and selectivity calculation method in the reported works.

Method	Conversion	Feed	Formula of $S(C_2H_4)$	Accuracy of $S(C_2H_4)$
A	$Conv = \frac{n_{C_2H_2,in} - n_{C_2H}}{n_{C_2H_2,in}}$	Without ethylene	$S_{C_2H_4} = \frac{n_{C_2H_4,out}}{n_{C_2H_4,out} + n_{C_2H_6,out} + 2n_{C_4,out}}$	Overrated due to the neglect of GO
B		With excess of ethylene	$S_{C_2H_4} = \frac{n_{C_2H_2,in} - n_{C_2H_2,out}}{n_{C_2H_2,in} - n_{C_2H_2,out} + n_{C_2H_6,out} + 2n_{C_4,ou}$	Overrated due to the equation and the neglect of GO
C		With excess of ethylene	$S_{C_2H_4} = 1 - \frac{n_{C_2H_6,out} - n_{C_2H_6,in} + 2(n_{C_4,out} - n_{C_4}}{n_{C_2H_2,in} - n_{C_2H_2,out}}$	Overrated due to the neglect of GO
D		With excess of ethylene	$S_{C_2H_4} = 1 - \frac{n_{C_2H_6,out} - n_{C_2H_6,in}}{n_{C_2H_2,in} - n_{C_2H_2,out}}$	Highly overrated due to the neglect of C_4 and GO
E		Without ethylene	$S_{C_2H_4} = \frac{n_{C_2H_4,out} - n_{C_2H_4,in}}{n_{C_2H_2,in} - n_{C_2H_2,out}}$	Accurate

Table S3. Comparison of Pd-Zn/SiO_2-t catalysts for acetylene hydrogenation.

Catalyst	Reaction *T*, °C	Con., %	S(C_2H_6), %	S(C_2H_4), %	S(C_4), %	S(GO), %
Pd-Zn/SiO_2-0	57	96	13	55	16	16
Pd-Zn/SiO_2-2	95	98	8	74	14	4
Pd-Zn/SiO_2-4	172	98	2	81	15	2

Table S4. Activation energy of butadiene formation on the Rh(111) and RhZn(110) surfaces (unit : eV)

	TS1	TS2	TS3
Rh(111)	0.46	0.58	0.40
RhZn(110)	0.66	0.61	1.40

Table S5. Free energy corrected for the temperature of ZnO(g), Zn(g), H_2(g) and H_2O(g) at 473, 573, 673 and 773 K.

	Temp (K)	ZPE (eV)	$H_{0\to T}$ (eV)	S (eV/K)	$G_{0\to T}$ (eV)
ZnO(gas)	473	0.046	0.20	0.00258	-1.02
	573	0.046	0.24	0.00265	-1.28
	673	0.046	0.27	0.00271	-1.55
	773	0.046	0.31	0.00276	-1.82
Zn(gas)	473	0.00	0.10	0.00177	-0.73
	573	0.00	0.12	0.00181	-0.91
	673	0.00	0.14	0.00184	-1.10
	773	0.00	0.17	0.00187	-1.28
H_2(gas)	473	0.27	0.41	0.00149	-0.30
	573	0.27	0.44	0.00155	-0.45
	673	0.27	0.47	0.00160	-0.61
	773	0.27	0.50	0.00164	-0.77
H_2O(gas)	473	0.56	0.73	0.00212	-0.27
	573	0.56	0.77	0.00219	-0.49
	673	0.56	0.80	0.00225	-0.71
	773	0.56	0.84	0.00231	-0.94

Table S6. Free energy changes $\Delta G_T(1)$, $\Delta G_T(2)$ and $\Delta G_T(3)$ corrected for the temperature.

Temp (K)	$\delta G_T(1)$ (eV)	$\Delta G_T(1)$ (eV)	$\delta G_T(2)$ (eV)	$\Delta G_T(2)$ (eV)	$\delta G_T(3)$ (eV)	$\Delta G_T(3)$ (eV)
0	0	4.82	0	1.14	0	-2.19
473	-1.02	3.81	-0.27	0.43	0.73	-1.46
573	-1.28	3.54	-0.49	0.18	0.91	-1.28
673	-1.55	3.28	-0.71	-0.06	1.10	-1.10
773	-1.82	3.00	-0.94	-0.31	1.28	-0.91

Details of the free energy calculation

The chemical equations are summarized as

(1) ZnO(221 slab) → ZnO(221 slab, with one ZnO row evaporated) + 2ZnO(gas)

(2) ZnO(221 slab) + 2H2(gas) → ZnO(221 slab, with one ZnO row evaporated) + 2Zn(gas) + 2H_2O(gas)

(3) Rh(221 slab) + Zn(gas) → Rh-Zn(221 slab, with one Zn row)

The model for equations (1) and (2) was established using the (221) surface of ZnO and one row of ZnO was evaporated from the step. Typically, in each slab, two Zn and two O atoms were evaporated.

Thus, the energy changes at 0 K (neglecting zero point energy (ZPE)) are:

$\Delta E_0(1) = (E_{\text{ZnO(221 slab, with one ZnO row evaporated)}} + 2E_{\text{ZnO(gas)}} - E_{\text{ZnO(221 slab)}})/2 = 4.82$ eV

$\Delta E_0(2) = (E_{\text{ZnO(221 slab, with one ZnO row evaporated)}} + 2E_{\text{Zn(gas)}} + 2E_{\text{H2O(gas)}} - E_{\text{ZnO(hydrogenated 221 slab)}} - 2E_{\text{H2(gas)}})/2 = 1.14$ eV

The model for equation (3) was established using the Rh(221) surface, and one row of Zn was formed at the step.

Thus, the energy changes at 0 K (neglecting ZEP) are:

$\Delta E_0(3) = E_{\text{Rh-Zn(221 slab, with one row Zn)}} - E_{\text{Rh(221 slab)}} - E_{\text{Zn(gas)}} = -2.19$ eV

The adjustment of Gibbs free energy of the gas components (Table S5) was calculated using the following equation:

$G_{0\to T} = H_{0\to T} - T \times S$

Thus, the Gibbs free energy of each chemical equation (Table S6) was

$\Delta G_T = G_{T,\text{ product}} - G_{T,\text{ reactant}} = \Delta E_0 + \delta G_T$

where,

$\delta G_T(1) = G_{0\to T}$(ZnO)

$\delta G_T(2) = G_{0\to T}(Zn) + G_{0\to T}(H_2O) - G_{0\to T}(H_2)$

$\delta G_T(3) = - G_{0\to T}(Zn)$

Reference

1. Wang, Y.; Liu, B.; Lan, X.; Wang, T., Subsurface Carbon as a Selectivity Promotor to Enhance Catalytic Performance in Acetylene Semihydrogenation. *ACS Catal.* **2021,** *11* (16), 10257-10266.
2. Kresse, G.; Furthmüller, J., Efficiency of ab-initio total energy calculations for metals and semiconductors using a plane-wave basis set. *Computational Mater. Sci.* **1996,** *6* (1), 15-50.
3. Kresse, G.; Furthmüller, J., Efficient iterative schemes for ab initio total-energy calculations using a plane-wave basis set. *Phys. Rev. B* **1996,** *54* (16), 11169-11186.
4. Blöchl, P. E., Projector augmented-wave method. *Phys. Rev. B Condens. Matter.* **1994,** *50* (24), 17953-17979.
5. Kresse, G.; Joubert, D., From ultrasoft pseudopotentials to the projector augmented-wave method. *Phys. Rev.B* **1999,** *59* (3), 1758-1775.
6. Perdew, J. P.; Burke, K.; Ernzerhof, M., Generalized Gradient Approximation Made Simple. *Phys. Rev. Lett.* **1996,** *77* (18), 3865-3868.
7. Henkelman, G.; Uberuaga, B. P.; Jónsson, H., A climbing image nudged elastic band method for finding saddle points and minimum energy paths. *J. Chem. Phys.* **2000,** *113* (22), 9901-9904.
8. Jain, A.; Ong, S. P.; Hautier, G.; Chen, W.; Richards, W. D.; Dacek, S.; Cholia, S.; Gunter, D.; Skinner, D.; Ceder, G.; Persson, K. A., Commentary: The Materials Project: A materials genome approach to accelerating materials innovation. *APL Mater.* **2013,** *1* (1), 011002.
9. Wang, V.; Xu, N.; Liu, J.-C.; Tang, G.; Geng, W.-T., VASPKIT: A user-friendly interface facilitating high-throughput computing and analysis using VASP code. *Comput. Phys. Commun.* **2021,** *267*, 108033.
10. Onda, A.; Komatsu, T.; Yashima, T., Characterization and catalytic properties of Ni–Sn intermetallic compounds in acetylene hydrogenation. *Phys. Chem. Chem. Phys.* **2000,** *2* (13), 2999-3005.
11. Komatsu, T.; Kishi, T.; Gorai, T., Preparation and catalytic properties of uniform particles of Ni_3Ge intermetallic compound formed inside the mesopores of MCM-41. *J. Catal.* **2008,** *259* (2), 174-182.
12. Osswald, J.; Kovnir, K.; Armbrüster, M.; Giedigkeit, R.; Jentoft, R. E.; Wild, U.; Grin, Y.; Schlögl, R., Palladium–gallium intermetallic compounds for the selective hydrogenation of acetylene: Part II: Surface characterization and catalytic performance. *J. Catal.* **2008,** *258* (1), 219-227.
13. Armbrüster, M.; Wowsnick, G.; Friedrich, M.; Heggen, M.; Cardoso-Gil, R., Synthesis and catalytic properties of nanoparticulate intermetallic Ga–Pd compounds. *J. Am. Chem. Soc.* **2011,** *133* (23), 9112-9118.
14. Armbrüster, M.; Kovnir, K.; Friedrich, M.; Teschner, D.; Wowsnick, G.; Hahne, M.; Gille, P.; Szentmiklósi, L.; Feuerbacher, M.; Heggen, M.; Girgsdies, F.; Rosenthal, D.; Schlögl, R.; Grin, Y., $Al_{13}Fe_4$ as a low-cost alternative for palladium in heterogeneous hydrogenation. *Nat. Mater.* **2012,** *11* (8), 690-693.
15. Zhou, H.; Yang, X.; Li, L.; Liu, X.; Huang, Y.; Pan, X.; Wang, A.; Li, J.; Zhang, T., PdZn intermetallic nanostructure with Pd–Zn–Pd ensembles for highly active and chemoselective semi-hydrogenation of acetylene. *ACS Catal.* **2016,** *6* (2), 1054-1061.
16. Luo, Y.; Alarcón Villaseca, S.; Friedrich, M.; Teschner, D.; Knop-Gericke, A.; Armbrüster, M., Addressing electronic effects in the semi-hydrogenation of ethyne by $InPd_2$ and intermetallic Ga–Pd compounds. *J. Catal.* **2016,** *338*, 265-272.
17. Liu, Y.; Liu, X.; Feng, Q.; He, D.; Zhang, L.; Lian, C.; Shen, R.; Zhao, G.; Ji, Y.; Wang, D.; Zhou, G.; Li, Y., Intermetallic Ni_xM_y (M = Ga and Sn) nanocrystals: a non-precious metal catalyst for semi-hydrogenation of alkynes. *Adv. Mater.* **2016,** *28* (23), 4747-4754.
18. Feng, Q.; Zhao, S.; Wang, Y.; Dong, J.; Chen, W.; He, D.; Wang, D.; Yang, J.; Zhu, Y.; Zhu, H.; Gu, L.; Li, Z.; Liu, Y.; Yu, R.; Li, J.; Li, Y., Isolated single-atom Pd sites in intermetallic nanostructures: high catalytic selectivity for semihydrogenation of alkynes. *J. Am. Chem. Soc.* **2017,** *139* (21), 7294-7301.
19. Cao, Y.; Zhang, H.; Ji, S.; Sui, Z.; Jiang, Z.; Wang, D.; Zaera, F.; Zhou, X.; Duan, X.; Li, Y., Adsorption site regulation to guide atomic design of ni–ga catalysts for acetylene semi-hydrogenation. *Angew. Chem. Int. Ed.* **2020,** *59* (28), 11647-11652.
20. Niu, Y.; Huang, X.; Wang, Y.; Xu, M.; Chen, J.; Xu, S.; Willinger, M.-G.; Zhang, W.; Wei, M.; Zhang, B., Manipulating interstitial carbon atoms in the nickel octahedral site for highly efficient hydrogenation of alkyne. *Nat. Commun.* **2020,** *11* (1), 3324.
21. Li, X.-T.; Chen, L.; Shang, C.; Liu, Z.-P., In situ surface structures of PdAg catalyst and their influence on acetylene semihydrogenation revealed by machine learning and experiment. *J. Am. Chem. Soc.* **2021,** *143* (16), 6281-6292.
22. Ge, X.; Ren, Z.; Cao, Y.; Liu, X.; Zhang, J.; Qian, G.; Gong, X.; Chen, L.; Zhou, X.; Yuan, W.; Duan, X., Enhanced acetylene semi-hydrogenation on a subsurface carbon tailored Ni–Ga intermetallic catalyst. *J. Mater. Chem. A* **2022,** *10* (37), 19722-19731.
23. Zhang, W.; Zhang, X.; Wang, J.; Ghosh, A.; Zhu, J.; LiBretto, N. J.; Zhang, G.; Datye, A. K.; Liu, W.; Miller, J. T., Bismuth-modulated surface structural evolution of Pd_3Bi intermetallic alloy catalysts for selective propane dehydrogenation and acetylene semihydrogenation. *ACS Catal.* **2022,** *12* (17), 10531-10545.
24. Ge, X.; Dou, M.; Cao, Y.; Liu, X.; Yuwen, Q.; Zhang, J.; Qian, G.; Gong, X.; Zhou, X.; Chen, L.; Yuan, W.; Duan, X., Mechanism driven design of trimer Ni_1Sb_2 site delivering superior hydrogenation selectivity to ethylene. *Nat. Commun.* **2022,** *13* (1), 5534.
25. Dasgupta, A.; He, H.; Gong, R.; Shang, S.-L.; Zimmerer, E. K.; Meyer, R. J.; Liu, Z.-K.; Janik, M. J.; Rioux, R. M., Atomic control of active-site ensembles in ordered alloys to enhance hydrogenation selectivity. *Nat. Chem.* **2022,** *14* (5), 523-529.
26. Guo, Q.; Chen, R.; Guo, J.; Qin, C.; Xiong, Z.; Yan, H.; Gao, W.; Pei, Q.; Wu, A.; Chen, P., Enabling semihydrogenation of alkynes to alkenes by using a calcium palladium complex hydride. *J. Am. Chem. Soc.* **2021,** *143* (49), 20891-20897.
27. Liu, S.; Li, Y.; Yu, X.; Han, S.; Zhou, Y.; Yang, Y.; Zhang, H.; Jiang, Z.; Zhu, C.; Li, W.-X.; Wöll, C.; Wang, Y.; Shen, W., Tuning crystal-phase of bimetallic single-nanoparticle for catalytic hydrogenation. *Nat. Commun.* **2022,** *13* (1), 4559.
28. Borodziński, A.; Bond, G. C., Selective hydrogenation of ethyne in ethene-rich streams on palladium catalysts. Part 1. effect of changes to the catalyst during reaction. *Catal. Rev.* **2006,** *48* (2), 91-144.
29. Borodziński, A.; Bond, G. C., Selective hydrogenation of ethyne in ethene-rich streams on palladium catalysts, Part 2: steady-state kinetics and effects of palladium particle size, carbon monoxide, and promoters. *Catal. Rev.* **2008,** *50* (3), 379-469.